Shape Transformation

DOI: 10.1002/ange.201303984

Polymeric Microtubules That Breathe: CO_2-Driven Polymer Controlled-Self-Assembly and Shape Transformation**

*Qiang Yan and Yue Zhao**

One of the most intriguing properties of natural phospholipid self-organized structures is their ability to readily change their shapes under physiological stimuli.[1] Numerous cell biological activities rely on these lipid bilayer deformable behaviors.[2] Considering the complexity of natural biomembranes, mimicking their deformable behaviors by use of synthetic molecules has become a long-term goal in many subdisciplines of chemistry.[3] Amphiphilic block copolymers, acting as a class of macromolecular building blocks, have spurred considerable interest in recent years because they possess diversiform and sophisticated self-assembled architectures in solution.[4] They are believed to be ideal candidates to imitate the shape transformation of those biomolecular aggregates. Several successful studies have demonstrated, by fluctuating environmental parameters such as osmosis, pH, temperature, light, redox, and shear force,[5–9] that block copolymer aggregates display stimuli-responsive biphase or multiphase transition. However, exogenous stimulation conditions that the majority of reports focused on probably cause potential side effects to biological cells, including incompatibility, cytotoxicity, membrane decomposition, and gene damage. Carbon dioxide (CO_2), as a key endogenous metabolite, can freely diffuse through cytomembranes and it plays an important role in regulating bilayer osmosis and constitution. Therefore, developing CO_2 as a new stimulus to construct responsive polymer assemblies holds great promise for cell mimicry. In this regard, some nascent effort has been made recently. Yuan and co-workers have shown that CO_2 can effectively adjust polymer vesicular sizes;[10] Zhao's group has showed that the micellization of block copolymers can be induced by CO_2 levels.[11] Beyond these discoveries, whether CO_2 is capable of stimulating polymeric shape transformation and modulating their self-assembly structures remains a momentous challenge.

Herein, we designed and synthesized an amidine-containing block copolymer (EAS), which consists of two asymmetric flanks of hydrophilic poly(ethylene oxide) (E) and hydrophobic polystyrene (S), and poly((*N*-amidine)dodecylacrylamide) as intermediate CO_2-sensitive bridging block (A). In aqueous solution, EAS can self-assemble into microscopic tubular architectures. By introducing CO_2 into this system, A blocks are gradually protonated by the acidic gaseous medium, leading to a successive variation of the hydrophilic–hydrophobic balance in the block. Once the polymer amphiphilicity has a small alteration, it might offer a driving force to reshape the aggregated structures.[12] Thus we speculated that by stepwise tuning of CO_2 levels, it is feasible to realize CO_2-driven polymer self-assembly and to further trigger a sequence of controlled shape transformation (Scheme 1).

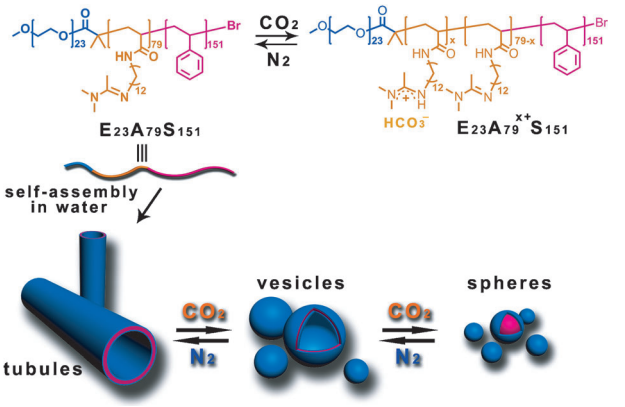

Scheme 1. Gas-switchable amidine-containing triblock copolymer EAS (top) and representation of its CO_2-driven controlled self-assembly and shape transformation behavior (bottom).

The copolymer EAS was prepared by sequential atom transfer radical polymerization,[13] which afforded a well-defined and near-monodisperse product ($E_{23}A_{79}S_{151}$, M_n = 42.5 kDa, M_w/M_n = 1.17; details of polymer synthesis and characterization are given in the Supporting Information). When it dissolved in selective solvents, an opaque colloidal solution resulted (THF/H_2O, 55:45 w/w, 4.0 mL). The strong Tyndall effect implies the formation of micellar particles. Gas responsivity was first studied by conductivity measurements.[14] With the addition of CO_2, the solution conductivity markedly rose from 3.6 to 31.1 μS cm^{-1}, accompanied by pH falling from 8.2 to 5.6, suggesting the protonation of copolymer chains to generate extra charge. Upon treatment with N_2, the original low conductivity could be restored owing to deprotonation. Reproducible cycles under alternating CO_2/N_2 stimuli confirmed the reversibility (Supporting Information, Figure S4).

We next targeted to explore whether the EAS aggregates can deform upon exposure to CO_2 atmosphere. As the size of

[*] Dr. Q. Yan, Prof. Dr. Y. Zhao
Département de Chimie, Université de Sherbrooke
Sherbrook, Quebec, J1K 2R1 (Canada)
E-mail: yue.zhao@usherbrooke.ca

[**] This work was financially supported by the National Basic Research Program of China (2009CB93060), the Natural Sciences and Engineering Research Council of Canada (NSERC), le Fonds Quebecois de la Recherche sur la Nature et les Technologies of Quebec (FQRNT).

Supporting information for this article is available on the WWW under http://dx.doi.org/10.1002/anie.201303984.

colloid particles has positive correlation to the solution turbidity, a time-resolved experiment was performed to detect the turbidity change within different CO_2 concentrations. To ensure the validity, we used a gas microflow pump to stabilize the aeration rate at about 1.0 mL min^{-1} and recorded data at a fixed time interval of 30 s. The work curve covers two fast-descent stages and three platform stages (Figure 1a): In

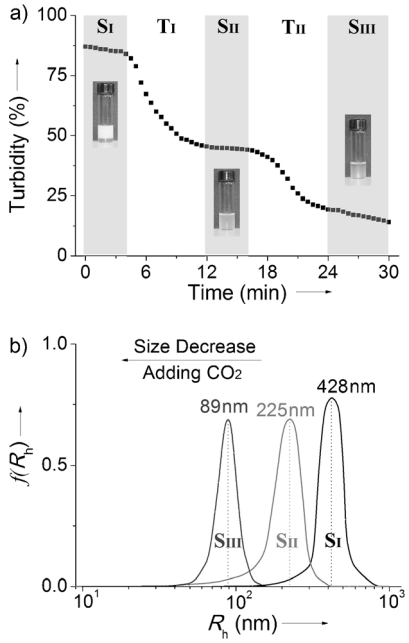

Figure 1. a) Turbidity changes of EAS aggregates under continuous CO_2 stimulation (Inset: pictures of the assemblies in solution in three different stages). b) DLS data for EAS aggregates in the presence of CO_2 with different stimulation times (S_I 0 min, S_{II} 15 min, S_{III} 25 min).

the time range of 0–4, 12–16, and 24–30 min, the turbidity remains steady at 87%, 45%, and 19%, respectively, which means that the variation of the micellar scales are negligible in these time ranges. In contrast, rapid reduction between each two adjacent platform stages (4–12 min, 87%→45%; 16–24 min, 45%→19%) suggests that the particle dimensions can undergo an extensive decrease. From this stepped decline curve, we extrapolated that each platform period (termed as S_I for 0–4 min, S_{II} for 12–16 min, and S_{III} for 24–30 min) might correspond to a certain stable phase of EAS aggregates, whereas each descending process (T_I for 4–12 min and T_{II} for 16–24 min) might correspond to a transitional state. Dynamic light scattering (DLS) results further supported this hypothesis (Figure 1b). In the absence of CO_2 stimulus (in the S_I stage), the average hydrodynamic radius R_h of EAS assemblies can reach up to 428 nm. However, when we applied CO_2 for 15 min in the S_{II} stage, these aggregates appeared an enormous shape shift, as indicated by the R_h reducing nearly by half down to 225 nm. Further entering into S_{III} (25 min), another sharp R_h diminution from 225 to 89 nm was clearly observed. Injecting N_2 can induce the R_h recovery (Supporting Information, Figure S5). Such a series of significant and reversible size changes reflect that the morphological differentiation of EAS is dependent on the CO_2 concentration.

To visualize the differences of EAS polymeric morphologies in various stages, we used transmission electron microscopy (TEM). As shown in Figure 2a, EAS copolymers

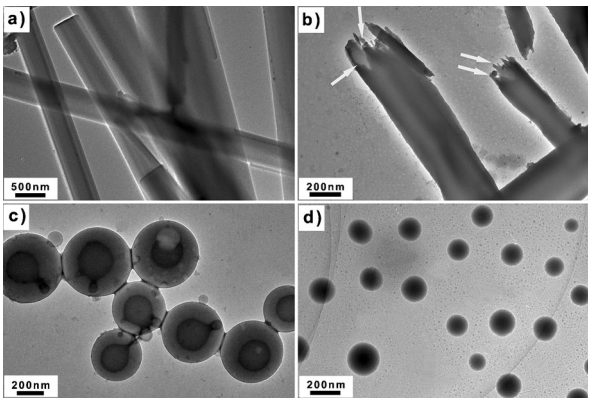

Figure 2. TEM images of EAS aggregates in different levels of CO_2 stimulus: a), b) no stimulus (S_I stage), c) 15 min (S_{II} stage), d) 25 min (S_{III} stage). Scale bars: a) 500 nm, b)–d) 200 nm.

can self-assemble into typical rod-like structures with no stimulus (also in the S_I stage). Determined by TEM automatic statistics (more than 55 objects), the diameter of these rigid aggregates ranges from 320 to 680 nm and their axial length is more than several micrometers. Their one-dimensional structures are in accordance with the equivalent radius of 428 nm from DLS. Further investigations revealed that these long rods are virtually polymer microtubules, as shown by the broken tubules: the clear contrast between the dark jagged edge and the gray central part discloses their hollow lumens (Figure 2b, indicated by arrows). These tubes kept in shape over three weeks when no stimulus was exerted. It is interesting that CO_2 gas activated unexpected phenomena. After bubbling CO_2 through the polymer solution for 15 min (in the S_{II} stage), the tubules completely vanished, and instead a great number of submicrometer vesicles with the average sizes of 410 nm were dominant in the solution (Figure 2c). Continuously purging with CO_2 for up to 25 min (in the S_{III} stage), their morphology underwent a further transformation. Nanoscaled spherical micelles were captured, and they exhibited well-defined core–corona structures with a near-uniform diameter of 158 nm (Figure 2d). These aggregated scales further decreased by 61%, consistent with the changing tendency in DLS experiments. The results indicate that CO_2 levels can modulate the curvature of the assemblies, resulting in multiple morphological transitions in a controllable manner.

From microtubules through intermediate vesicles and ultimately to nanosized globular micelles, this process can be considered as CO_2-driven shape transformation. To further elucidate this viewpoint, the detailed changes of the EAS aggregates were tracked in real time. Optical microscopic images showed that adding CO_2 for 4 min, a handful of long microtubules (S_I, Figure 3a) began to fracture into small vesicular objects (indicated by arrows in Figure 3b). If the bubbling time was extended to 8 min, corresponding to the T_I

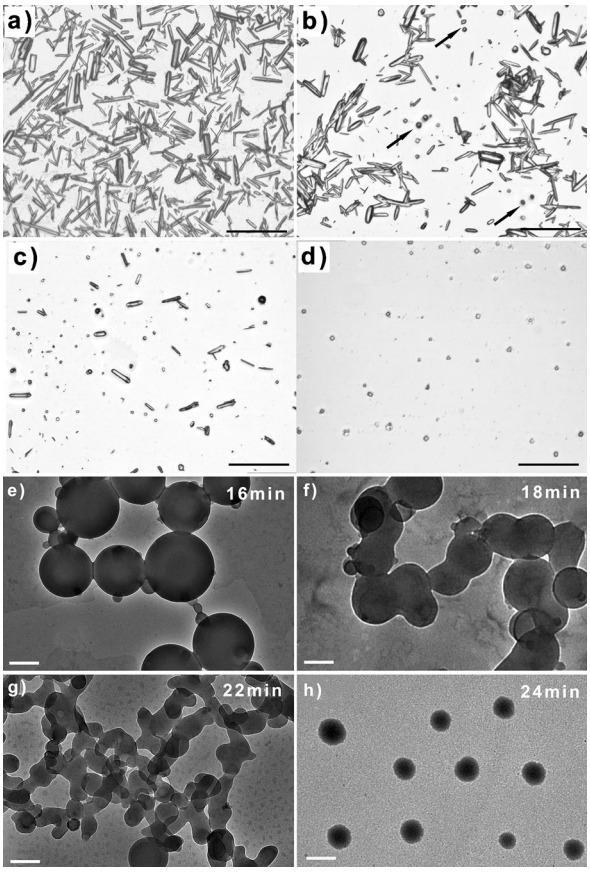

Figure 3. Morphological evolution of EAS aggregates tuned by CO_2 at various gas stimulus times. a)–d) Optical microscopic images (scale bar 25 μm): a) 0 (S_I), b) 4 (T_I), c) 8 (T_I), d) 12 min (S_{II}). e)–h) TEM images (scale bar 200 nm): e) 16 (S_{II}), f) 20 (T_{II}), g) 22 (T_{II}), h) 24 min (S_{III}).

stage, the quantity of vesicles increased at the expense of the tubular aggregates (Figure 3c). It is likely that these vesicles were produced from the fission of those original tubules. When CO_2 was passed through the solution for 12 min, the vesicles occupied the main phase and stabilized for ~4 min, as confirmed by TEM (S_{II}, Figure 3d,e). During the second transitional stage (T_{II}), these vesicles slightly contracted and showed membrane adhesion. With prolongation of aeration time, their sizes further decreased, accompanied with the membrane fusion and connection to form aggregates with the appearance of a string of beads (Figure 3f,g).[15] Finally, in the stable state of S_{III}, these beads constricted themselves and separated into the smaller spheres (Figure 3h).[15] Furthermore, it seemed there is a "saturation" point: the micellar morphology no longer changed with further increasing the CO_2 stimulation to 50 min (Supporting Information, Figure S6). The entire transformation is manipulated by CO_2, which is in many ways reminiscent of a breathing deformable motion.[16] The tubular and micellar morphology can be identified as the beginning and end of this breathing motion.

After figuring the procedure, we attempted to understand the mechanism on how CO_2 drives the morphology change and shape transformation of the aggregates. In general, the aggregate geometry of the block copolymer amphiphiles can be predicted based on the concept of the hydrophilic–hydrophobic ratio of Discher et al.:[12] the hydrophilic mass fraction, f_{philic} ($0 < f_{philic} < 1$), dictates the shape of polymer aggregates to some extent. It can be calculated by $f_{philic} = \Sigma N_{philic} m_{philic} / (\Sigma N_{philic} m_{philic} + \Sigma N_{phobic} m_{phobic})$, where the m_i is monomer mass that establish the total molecular weight of the polymer and N_i is repeating unit number. The block copolymers are theoretically expected to form spherical micelles when $f_{philic} > 50\,\%$, worm-like micelles when $40\,\% < f_{philic} < 50\,\%$, vesicles for $25\,\% < f_{philic} < 40\,\%$, and planar structures for $f_{philic} < 25\,\%$. In our polymer system, in the absence of CO_2 (in the S_I stage), the E block is the only hydrophilic portion for which f_{philic} is estimated to by about 2.4% (Supporting Information, Table S1). When CO_2 is added for 15 min (in the S_{II} stage), A block can be partially protonated to A^+, which causes the f_{philic} to increase to 25%. Prolonging the aeration time to 30 min (in the S_{III} stage), the protonation is further amplified. Higher N_{A+} results in an increase of f_{philic} up to 46%. During the three stable states (S_I, S_{II}, and S_{III}), f_{philic} grew from 2.4% through 25% to 46%, approximately corresponding to tubular, vesicular, and spherical shape, respectively. Considering that the A^+ block is polyelectrolyte and has stronger hydration effect than a non-charged hydrophilic block like E, the slight discrepancy between theoretical and calculated values is understandable.

On the other hand, the aggregate surface charge (ζ) detected by Zeta potentiometer and the average aggregated number (N_{agg}) by static light scattering further corroborate the deformable mechanism (Supporting Information, Figure S7 and Table S2). Owing to strong phase separation among the three blocks, the initial tubular assemblies should be composed by a three-layer structure in which S blocks act as the hydrophobic core, hydrophilic E blocks stretch outwardly and inwardly as the corona, and A blocks are sandwiched in the middle. Their lowest curvature is attributed to the weak chain interactions and the compact chain arrangement (Figure 4, S_I). However, in the S_{II} stage, CO_2 induced part of amidine pendants to be protonated and transformed to amidinium species; as a result, the charged A^+ blocks extruded to form a new corona, but uncharged blocks were still entrapped into the core. Before and after CO_2 was injected, the Zeta potential (ζ) changed from −6.9 mV to +20.3 mV, indicating an increase in the surface positive charge. Meanwhile, the N_{agg} showed a sharp decrease from 2.58×10^6 to 4.02×10^4. The results indicate that to counterbalance the increasing electrostatic repulsion among the corona chain, each tubular object is forced to reduce its volume, adopting a higher curvature to optimize interfacial free energy. Thus, the microtubules started to break up into the smaller vesicles (Figure 4, S_{II}). Bubbling CO_2 to enter into S_{III} stage, the surface potential further increased to $\zeta = +31.6$ mV and N_{agg} decreased 27 times to 1.47×10^3, facilitating the assemblies to expand their chain spacing to minimize the corona repulsions. Therefore, these vesicles finally divided into the smallest spheres for maximizing their curvature (Figure 4, S_{III}). However, because CO_2 is a weak acid, even though CO_2 is continually injected into the solution within 50 min, the protonation of A blocks will stop at the solution pH corresponding to CO_2 saturated concentration (pH 5.6). It

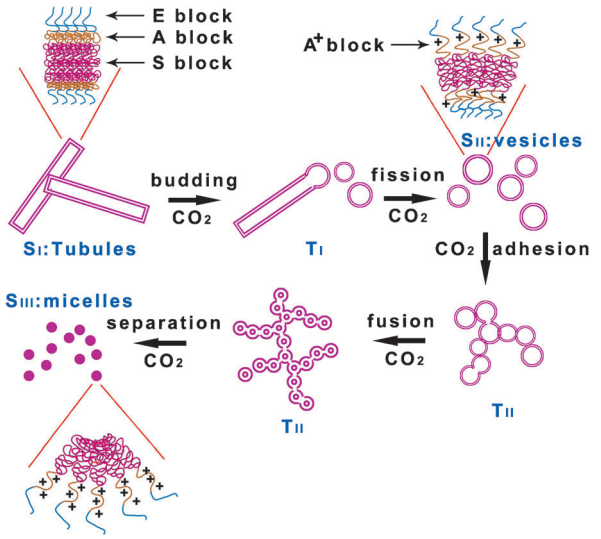

Figure 4. Representation of the CO_2-driven self-assembly process and successive shape evolution of EAS aggregates.

is the reason that the spherical micelles cannot further change their shape.

In conclusion, we have developed a gas-sensitive triblock copolymer that exhibits CO_2-driven controlled self-assembly and transformation over a broad range of sizes and shapes. The gas-regulated and successive deformation from microscopic tubules breathing into submicroscopic vesicles and nano-micelles successfully mimics the evolution of some living cells and organelles. Through modulating the CO_2 levels to tune the copolymer hydrophilic–hydrophobic ratio, the interfacial curvature and geometry of the self-assembled polymer aggregates can be precisely controlled. It is anticipated that the polymer model could open up a new door to building "living" assemblies for cell mimicry.

Received: May 9, 2013
Revised: June 18, 2013
Published online: August 8, 2013

Keywords: biomimics · block copolymers · carbon dioxide · controlled self-assembly · shape transformation

[1] a) D. P. Gilbert, P. De Camilli, *Nature* **2006**, *443*, 651–657; b) Y. F. Zhou, D. Y. Yan, *Angew. Chem.* **2005**, *117*, 3287–3290; *Angew. Chem. Int. Ed.* **2005**, *44*, 3223–3226.

[2] a) G. K. Voeltz, T. A. Rapoport, *Cell* **2006**, *124*, 573–586; b) G. K. Voeltz, M. M. Rolls, T. A. Rapoport, *EMBO Rep.* **2002**, *3*, 944–950.

[3] a) K. Farsad, P. De Camilli, *Curr. Opin. Cell Biol.* **2003**, *15*, 372–381; b) Y. F. Zhou, D. Y. Yan, *J. Am. Chem. Soc.* **2005**, *127*, 10468–10469; c) K. T. Kim, J. H. Zhu, S. A. Meeuwissen, J. J. L. M. Cornelissen, D. J. Pochan, R. J. M. Nolte, J. C. M. van Hest, *J. Am. Chem. Soc.* **2010**, *132*, 12522–12524; d) D. A. Wilson, R. J. M. Nolte, J. C. M. van Hest, *Nat. Chem.* **2012**, *4*, 268–274.

[4] a) T. Smart, H. Lomas, M. Massignani, M. V. Flores-Merino, L. R. Perez, G. Battaglia, *Nano Today* **2008**, *3*, 38–46; b) D. E. Discher, A. Eisenberg, *Science* **2002**, *297*, 967–973; c) R. C. Hayward, D. J. Pochan, *Macromolecules* **2010**, *43*, 3577–3584.

[5] a) J. Z. Du, S. P. Armes, *J. Am. Chem. Soc.* **2005**, *127*, 12800–12801; b) J. Rodríguez-Hernández, S. Lecommandoux, *J. Am. Chem. Soc.* **2005**, *127*, 2026–2027; c) K. E. B. Doncom, C. F. Hansell, P. Theato, R. K. O'Reilly, *Polym. Chem.* **2012**, *3*, 3007–3015.

[6] a) C. Pietsch, U. Mansfeld, C. Guerrero-Sanchez, S. Hoeppener, A. Vollrath, M. Wagner, R. Hoogenboom, S. Saubern, S. H. Thang, C. Remzi Becer, J. Chiefari, U. S. Schubert, *Macromolecules* **2012**, *45*, 9292–9302; b) Y. Cai, K. B. Aubrecht, R. B. Grubbs, *J. Am. Chem. Soc.* **2011**, *133*, 1058–1065; c) Y. T. Li, B. S. Lokitz, C. L. McCormick, *Angew. Chem.* **2006**, *118*, 5924–5927; *Angew. Chem. Int. Ed.* **2006**, *45*, 5792–5795; d) S. Hocine, A. Brulet, L. Jia, J. Yang, A. D. Cicco, L. Bouteiller, M. H. Lin, *Soft Matter* **2011**, *7*, 2613–2623; e) A. O. Moughton, J. P. Patterson, R. K. O'Reilly, *Chem. Commun.* **2011**, *47*, 355–357.

[7] a) S. K. M. Nalluri, B. J. Ravoo, *Angew. Chem.* **2010**, *122*, 5499–5502; *Angew. Chem. Int. Ed.* **2010**, *49*, 5371–5374; b) X. K. Liu, M. Jiang, *Angew. Chem.* **2006**, *118*, 3930–3934; *Angew. Chem. Int. Ed.* **2006**, *45*, 3846–3850; c) J. Q. Jiang, X. Tong, Y. Zhao, *J. Am. Chem. Soc.* **2005**, *127*, 8290–8291.

[8] a) H. Kim, S.-M. Jeong, J.-W. Park, *J. Am. Chem. Soc.* **2011**, *133*, 5206–5209; b) A. Napoli, M. Valentini, N. Tirelli, M. Müller, J. A. Hubbell, *Nat. Mater.* **2004**, *3*, 183–189; c) K. N. Power-Billard, R. J. Spontak, I. Manners, *Angew. Chem.* **2004**, *116*, 1280–1284; *Angew. Chem. Int. Ed.* **2004**, *43*, 1260–1264; d) J. H. Ryu, R. Roy, J. Ventura, S. Thayumanavan, *Langmuir* **2010**, *26*, 7086–7092; e) N. Ma, Y. Li, H. P. Xu, Z. Q. Wang, X. Zhang, *J. Am. Chem. Soc.* **2010**, *132*, 442–443.

[9] C.-W. Wang, D. Sinto, M. G. Moffitt, *ACS Nano* **2013**, *7*, 1424–1436.

[10] Q. Yan, R. Zhou, C. K. Fu, H. J. Zhang, Y. W. Yin, J. Y. Yuan, *Angew. Chem.* **2011**, *123*, 5025–5029; *Angew. Chem. Int. Ed.* **2011**, *50*, 4923–4927.

[11] a) D. Han, X. Tong, O. Boissiere, Y. Zhao, *ACS Macro Lett.* **2012**, *1*, 57–61; b) B. Yan, D. Han, O. Boissiere, P. Ayotte, Y. Zhao, *Soft Matter* **2013**, *9*, 2011–2016.

[12] a) B. M. Discher, Y.-Y. Won, D. S. Ege, J. C.-M. Lee, F. S. Bates, D. E. Discher, D. A. Hammer, *Science* **1999**, *284*, 1143–1146; b) D. E. Discher, F. Ahmed, *Annu. Rev. Biomed. Eng.* **2006**, *8*, 323–341; c) S. M. Loverde, V. Ortiz, R. D. Kamien, M. L. Klein, D. E. Discher, *Soft Matter* **2010**, *6*, 1419–1425.

[13] N. V. Tsarevsky, K. Matyjaszewski, *Chem. Rev.* **2007**, *107*, 2270–2299.

[14] Y. X. Liu, P. G. Jessop, M. Cunningham, C. A. Eckert, C. L. Liotta, *Science* **2006**, *313*, 958–960.

[15] C. Sanson, J.-F. Meins, C. Schatz, A. Soum, S. Lecommandoux, *Soft Matter* **2010**, *6*, 1722–1730.

[16] S. Y. Yu, T. Azzam, I. Rouiller, A. Eisenberg, *J. Am. Chem. Soc.* **2009**, *131*, 10557–10566.